López, JJ.; García Martínez, A.; Monsalve-Serrano, J.; Vielmo-Cogo, V.; Wittek, K. (2020). Potential of a Two-Stage Variable Compression Ratio Downsized Spark Ignition Engine for Passenger Cars under different driving conditions. Energy Conversion and Management. 203:1-15. https://doi.org/10.1016/j.enconman.2019.112251

Potential of a Two-Stage Variable Compression Ratio Downsized Spark Ignition Engine for Passenger Cars under different driving conditions

J. Javier López[a], Antonio García[a], Javier Monsalve-Serrano[a,*], Vitor Cogo[a] and Karsten Wittek[b]

[a]CMT - Motores Térmicos, Universitat Politècnica de València, Camino de Vera s/n, 46022 Valencia, Spain

[b]Mechanical Engineering Department, Heilbronn University, Germany

Energy Conversion and Management
Volume 203, 1 January 2020, 112251
https://doi.org/10.1016/j.enconman.2019.112251

Corresponding author (*):
Dr. J. Monsalve-Serrano (jamonse1@mot.upv.es)
Phone: +34 963876559
Fax: +34 963877650

Abstract

With the aim of reducing pollutant emissions from internal combustion engines (ICE), the application of stoichiometrically operated spark ignition (SI) engines, for light-duty vehicles, has been overcoming the compression ignition (CI) engines market share throughout the past years. The ability of a substantial reduction of the primary harmful emissions (HC, CO, and NOx) through the use of the simple three-way catalyst (TWC) is the main reason for that. Nonetheless, with increasing attention to CO_2 emissions, the development of highly efficient downsized SI engines turn to be of enormous interest. The synergies of multiple systems such as direct injection, turbocharger, and variable valve actuation are able to lead the SI efficiencies closer to those of CI engines. However, to enable high load operation on such downsized engines, the compression ratio (CR) must be reduced due to knock limitations, reducing the partial-load operations efficiency. The implementation of two-stage variable compression ratio (VCR) systems enables the extraction of high thermal efficiency with high CR at lower loads and extended knock-free high load operation with low CR. In this study, the evaluation of a two-stage VCR system applied to a state-of-the-art downsized SI engine was made through standard driving cycle simulations. The VCR mechanism is composed of an eccentric element in the small end of the connecting rod, which is rotated to increase/decrease the effective connecting rod length, achieving the CRs of 12.11:1 and 9.56:1. The engine was run in an eddy-current dynamometer test bench throughout the essential operating range to obtain the brake specific fuel consumption (BSFC) map. The VCR mechanism CR switching delay was also experimentally characterized to derive a function of the operating conditions. The measured map was entered into the map-based driving cycle simulation with a sub-model to account for the isolated effects of the transient period encompassing the compression ratio switching. The results show that slow CR transitions lead to fuel consumption penalties, which suggests the need for optimizing the control strategies of the VCR system. Even though this penalty, once the gear up-shift speed is optimized for each driving cycle, the VCR system still enables fuel

consumption reductions up to 3% on the WLTC driving cycle, up to 4% on the proposed urban driving cycles and up to 3% on highway driving cycles with respect to the fixed CR.

Keywords
Variable compression ratio; Downsized internal combustion engines; Fuel consumption; Driving cycles

1. Introduction

Since the Dieselgate scandal [1] a few years ago, the look over internal combustion engines (ICE) has had a sudden change. A great effort has been made to the development and reduction of emissions from diesel engines [2,3]. Through the development of high-pressure common-rail injection systems [4], advanced turbocharging technologies [5], aftertreatment systems [6,7], cold start strategies [8], alternative fuels [9], and advanced combustion modes [10,11]. Nonetheless, gasoline engines started occupying a growing market share of new passenger cars, as presented in Figure 1, mainly favored by the use of the simple and relatively inexpensive aftertreatment system, the three-way catalyst (TWC) [12]. The TWC can effectively reduce the primary combustion noxious emissions (HC, CO, and NOx) in stoichiometrically operated engines [13,14]. However, these engines have the handicap of intake throttling at partial-load conditions to maintain the stoichiometric air/fuel ratio, which induces high pumping and efficiency losses [15].

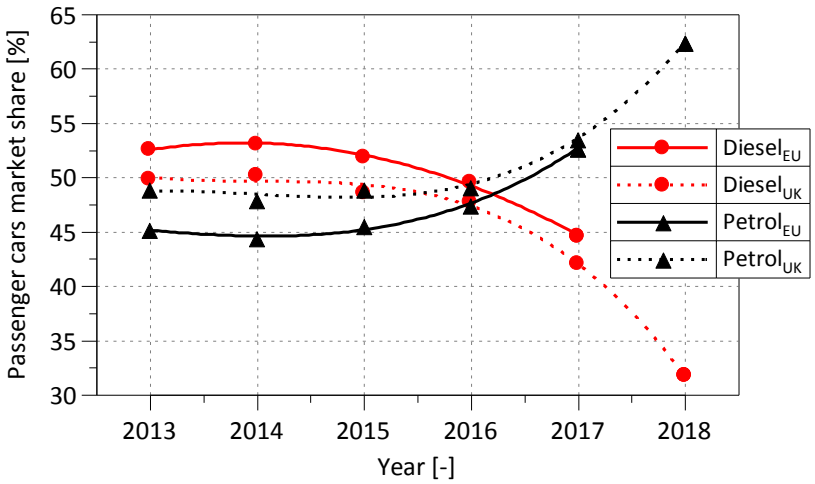

Figure 1 - Passenger cars market share in the European Union [16] and the United Kingdom [17].

With an increased look over CO_2 emissions reduction, the European Union (EU) set targets of 95 g CO_2/km (based on the New European Driving Cycle – NEDC) for the average passenger car fleet at 2021, counting on further reductions of 15% in 2025 and 37.5% in 2030 [18]. Therefore, for SI engines, the fuel efficiency improvement is the driver field of study [19]. The engine downsizing concept came intending to reduce the part-load losses through de-throttling using a smaller displaced volume. Therefore, the engine must be operated at higher mean effective pressure levels, employing turbocharger, to achieve the same torque as a naturally aspirated engine with bigger displacement [20]. However, at higher load levels, the autoignition induction time in the unburned charge is reduced, thus increasing the knock tendency [21]. Standard measures to diminish the knocking tendency are the spark retard or fuel enrichment, both decreasing the charge reactivity [22].

Moreover, some technologies have emerged to help mitigate the knock phenomena, allowing combustion to be optimally phased and reduce the use of over-fueling. Examples of these technologies are: the charge cooling by means of the fuel vaporization with single direct injection (DI) [23], split DI [24] or water injection [25], and charge dilution using cooled exhaust gas recirculation (EGR) [26]. Notwithstanding, the compression ratio (CR) plays the most crucial role in the trade-off between the knock limit and thermal efficiency. For that, the CR is commonly reduced up to two points in downsized turbocharged SI engines with respect to naturally aspirated ones [27], penalizing mainly the throttled operation efficiency. Variable compression ratio (VCR) systems have been originated to overcome such handicap, enabling increased partial-load efficiencies (with higher CRs) and knock-free high-load operation (with lower CRs).

Furthermore, the use of renewable fuels has been widely spread as additives or substitutes to gasoline due to the reduction of the carbon footprint [28]. In countries like Brazil, where ethanol is available at the petrol station as a full substitute to gasoline (which is already blended with ethanol owing to its anti-knock resistance) [29], the employment of flexible fuel engines is dominant on the market. However, the optimum fixed CR cannot be reached for the ethanol use on such engines, limited by the lower octane number of the gasoline. With the application of VCR systems, an optimum CR for the high-octane fuel could be exploited, resulting in a more effective use of both fuels.

The development of VCR systems is not a new subject [30]. However, the small penetration in series production indicates the complexity of its application, mainly due to the high number of moving parts or the intense modifications of the existing engine architecture and production line. Wittek et al. [31] proposed the classification of VCR systems into three major categories: 1) unconventional cranktrains (containing additional parts) [32,33], 2) variable crankshaft to cylinder head distance (changing the geometry of structural components) [34], and 3) variable kinematic lengths (changing the geometry of the crankshaft, pistons or connecting rods on a fixed geometry engine) [35,36]. The two-stage VCR system applied in this work is based on a variable-length connecting rod [37], which provides a simple solution to the VCR application problems. The connecting rod is composed of a movable eccentric small end, actuated by two hydraulic cylinders, elongating or shortening the effective connecting rod length. The hydraulic cylinders are actuated through a 3-port/2-way valve assembled on the big end of the connecting rod.

Numerous studies have already provided an idea of the fuel consumption benefits by using two-stage or multi-stage VCR systems with driving cycles simulation. Kleeberg et al. [38] found a fuel consumption benefit of around 5 to 7% considering a two-stage VCR system with low CR of 10 and high CR of 14 through the FTP-75 driving cycle simulation. Shelby et al. [39] estimated a fuel consumption reduction of up to 3.1% for a two-stage VCR system and 3.3% for a continuously VCR system on the EPA Metro-Highway cycle simulation. Boretti et al. [40] presented a fuel economy of 12.7%, modeling a two-stage VCR from 9.5:1 to 15:1 at the NEDC driving cycle. These studies apply operating maps based on two or more CRs maps, where the considered CR is the one with the smallest brake specific fuel consumption (BSFC) for each operating condition [41].

The same methodology to obtain the desired operating map was used in the present work. However, for driving cycle simulations, the use of the optimum operating map indicated previously, assumes that the VCR mechanism enables instantaneous CR switching, which is undoubtedly not true. For this reason, the CR switching times have been experimentally characterized, and a transient CR switching time function has been obtained. The function was applied in the framework of map-based driving cycle simulation to derive a fuel consumption evaluation of the transient switching VCR system. With this, a fair comparison between the fixed CR, the instantaneous switching VCR, and the transient/non-ideal VCR system was made.

The present work is structured as follows: first, the experimental methodology and instrumentation implemented to obtain the operation maps of the engine are presented. Later, the numerical methodology is explained, presenting the vehicle model and specifications, the tested driving cycles, the transient VCR model and controller, and the transition time function setup. Next, the results are divided into three subsections: results for urban driving cycles, highway driving cycles, and overall results. Finally, the conclusions of the work are presented.

2. Experimental methodology

This section describes the main characteristics of the test cell used in this study, focusing on the engine unit and the different systems of which is equipped, with a particular focus on the VCR system. Moreover, some considerations about the methodology followed during the experimental tests are provided.

2.1. Test engine

The use of steady-state map-based driving cycle simulations is a flexible tool to perform comparative studies between different engine operating parameters [42,43]. This methodology allows achieving consistent results in terms of fuel consumption and emissions analysis, with errors below 5% compared to the experimental data [44]. The experimental data used in the present study were obtained using a 3-cylinder turbocharged DISI Ford Ecoboost 1.0 liter engine, which represents a state-of-the-art downsized gasoline engine. The engine is provided of intake and exhaust cam phasers, four-valves per cylinder, pent-roof combustion chamber, and centrally mounted DI injector. Other relevant engine features are presented in Table 1. The engine also featured a prototype VCR connecting rod (Figure 2 (b)), such as presented in [45]. By actuating a hydraulic switching valve (mounted on the bottom of the connecting rod), the hydraulic cylinders are displaced, promoting the angular displacement of an eccentric part on the small end of the connecting rod. Accordingly, the connecting rod features two different effective lengths, thus two different compression ratios, without changing the displaced volume.

Table 1. Main engine specifications.

Configuration	Low CR	High CR
Number of cylinders	3	
Bore / Stroke	71.9 mm / 82 mm	
Compression ratio	9.56:1	12.11:1
Connecting rod length	134.8 mm	137 mm
Maximum tested BMEP	2.6 MPa	2.0 MPa
Maximum power	88 kW @ 6000 rpm (series engine)	

With the presented VCR system, only some minor modifications (other than the connecting rods) are necessary to be made on the original engine. The pistons were modified to account for the increased CR while staying with the original connecting rod length (at high CR). Thus, the piston bowl volume is reduced to keep the same clearance height and valve pocket volume. The addition of a servo-motor and a cam disc to actuate the CR switching valves within the oil reservoir is also necessary. For more details on the working principle of this VCR system, the reader is referred to [31].

2.2. Instrumentation and test procedure

The scheme presented in Figure 2 (a) shows the test-bench facility. An Eddy-current brake was used to maintain a constant engine speed. The engine operating parameters were managed through a Schaeffler type PROtroniC free programmable ECU. A closed-loop lambda control was used to maintain stoichiometric conditions throughout the entire operating map. The engine torque was manually changed through the intake pressure utilizing either throttle or wastegate valves. Intake and coolant temperatures were maintained at 35°C and 85°C for all the tested points using a liquid-to-air and liquid-to-liquid external heat exchangers, respectively. Therefore, all the driving cycle simulations presented in this work were considered to be in warm conditions. Other parameters such as the fuel injection pressure, injection timing, intake and exhaust cam phaser positions were manually kept at the same calibration values for both compression ratios. The engine oil was not externally conditioned.

The engine torque (measured with a torque flange HBM type T40B (500 Nm)), static pressures in the intake and exhaust manifolds (measured with a Keller type PAA-33X absolute pressure transducers), fuel and oil static pressures (measured with a Keller type PR-33X relative pressure transducers) were sampled at 1 kHz and averaged over 20 seconds at each measurement point. Standard European gasoline RON95 was delivered to the high-pressure fuel pump at 15°C and 0.4 MPa, and the mass flow rate was measured by an AVL type 733S dynamic fuel balance. The air-to-fuel excess ratio (λ) was measured with a wide-band Bosch type LSU 4.2 lambda sensor. The engine-out emissions were sampled downstream from the turbine with a Horiba type EXSA 1500L with a heated sampling line. Measured temperatures, fuel consumption, and emissions were sampled at 10 Hz and averaged over 20 seconds for each measurement point.

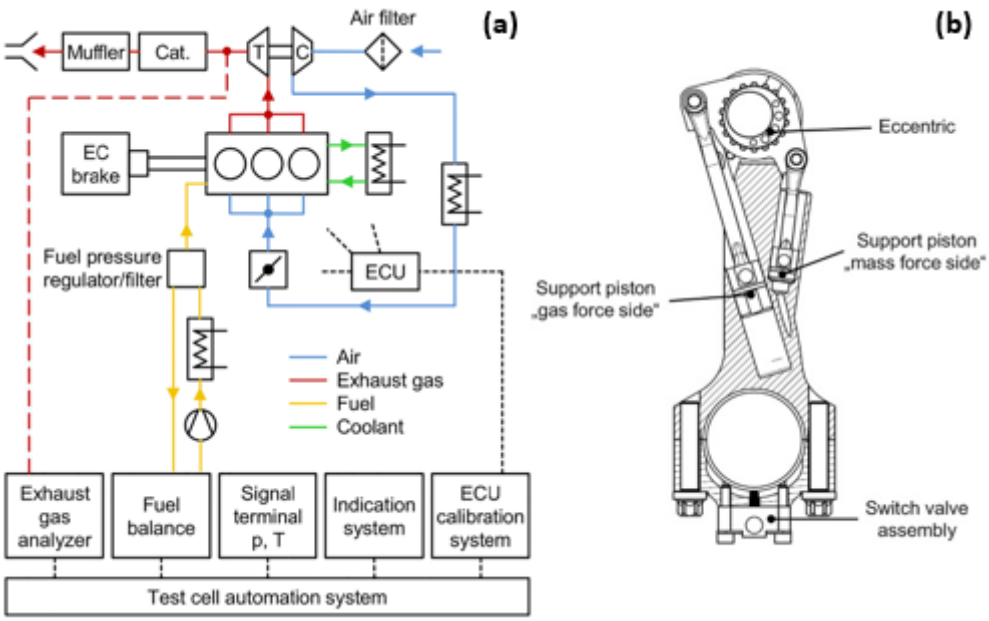

Figure 2 – (a): Test-bench scheme, (b): VCR connecting rod mechanism.

The in-cylinder pressure was acquired at each cylinder with Kistler type 6041BS31 water-cooled piezo-electric transducers, and their signals were amplified with Kistler type 5064C22 charge amplifiers. Absolute piezo-resistive Kistler type 4045A5V200S transducers were added to the intake (used for in-cylinder pressure pegging) and exhaust ports of the third cylinder. All the indicated measures were synchronized by means of a 720 pulses per revolution angular encoder Kistler type 2614CK1 with geometrical TDC position correction by TDC probe Kistler type 2629. All the indicated data were recorded along 200 consecutive cycles in a FEV type FEVIS.SY.2 indicating system.

For this study, the specific fuel consumption of the engine operated throughout the entire base engine map was measured at the two proposed compression ratios to provide data for the VCR concept evaluation during the driving cycles simulation. Although the maximum operable engine speed is 6000 rpm, the tests were performed ranging from 1000 to 4000 rpm, with an increment of 500 rpm, which represents regular operation for driving cycles. At each engine speed, a BMEP sweep was performed from 0.2 MPa up to limiting conditions, with an increment of 0.2 MPa. The spark advance was manually set to position the center of combustion, 50% of mass fraction burned (the values of which were derived from the Rassweiler/Withrow approximations [46]), at 8 degrees after the TDC, whenever possible. The maximum spark advance was limited by knocking conditions meanwhile the maximum spark retard was limited to conditions where the center of combustion reached 30 degrees after TDC or the exhaust temperature before the turbine or in the catalyst reached 950°C — resulting in 59 measured operating points for high CR and 73 operating points for low CR.

Initially, the engine was operated at moderate load and speed conditions for 30 minutes, to ensure warm conditions. The measurement points (speed and load) were set up and were only measured when stable conditions for temperatures and pressures (for oil, cooling water, intake, and exhaust) were reached. Each point was measured once (and repeated if necessary), and a reference point was measured three times

throughout the BMEP sweep procedure (at the beginning, in the middle, and at the end) to ensure data repeatability.

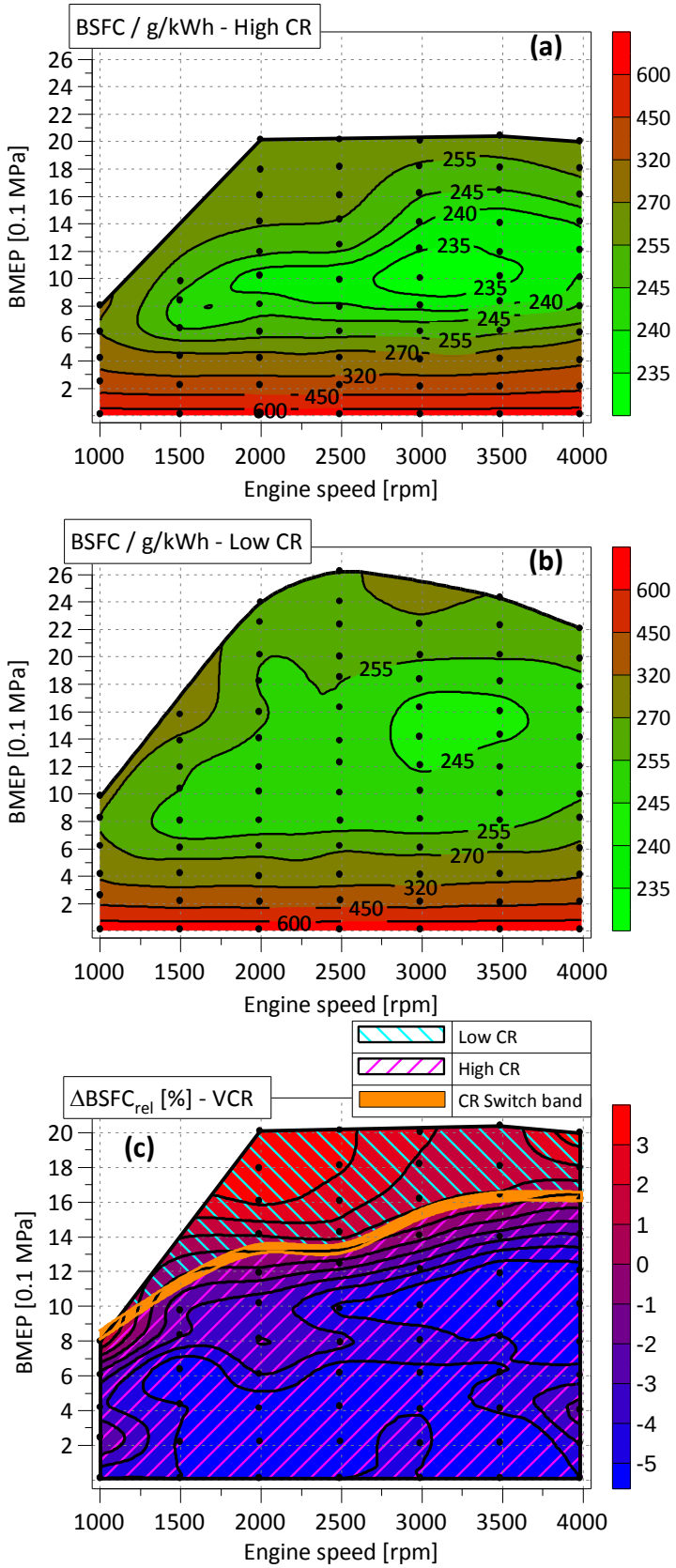

Figure 3 - Measured BSFC maps (a): high CR (12.11:1), (b): low CR (9.56:1), (c): High CR relative BSFC difference (with respect to, w.r.t., Low CR).

Through the uncertainty analysis, performed in [45], based on the theory of error propagations [47], the averaged BSFC measure uncertainty was around 2% for BMEP values higher than 0.4 MPa and around 3% below BMEP values of 0.4 MPa due to higher cyclic variability. The BSFC results for each compression ratio are presented in Figure 3 (a): high CR, (b): low CR, and (c): the relative difference of BSFC.

3. Numerical methodology

This section is divided into four subsections. First, the vehicle specifications and numerical models required to simulate the vehicle behavior are explained. Second, the different driving cycles considered in the study are described. Third, the bases of the VCR transient model and controller are explained. Finally, the details of the switching time function of the VCR system are presented.

3.1. Vehicle specifications and numerical models

A Ford Fiesta was used as vehicle for the driving cycle simulations. It is a subcompact (Class B) passenger car, equipped with the internal combustion engine described in the subsection 2.1. The OEM vehicle has a 5-gear manual transmission coupled to the engine and the differential coupled to the front wheels. The vehicle specifications are presented in Table 2. For comparison purposes, the fixed CR engine was considered to be the VCR at the low compression ratio (9.56:1). In spite of the OEM engine has a CR of 10:1, the results for both setups are mostly the same, as presented in [45].

Table 2. Main vehicle data.

Vehicle type [-]	OEM
Base vehicle Mass [kg]	1016
Passenger and Cargo Mass [kg]	100
Fuel Mass [kg]	45
Vehicle Drag Coefficient [-]	0.328
Frontal Area [m²]	2.14
Tires Size [mm/%/inch]	195/55/R15
Differential ratio [-]	3.61
1st gear ratio [-]	3.583
2nd gear ratio [-]	1.926
3rd gear ratio [-]	1.206
4th gear ratio [-]	0.878
5th gear ratio [-]	0.689

The driving cycle simulations were performed with GT-Suite (v2019, Gamma Technologies, LLC., Westmont, IL, USA), 0D vehicle model. The model has separate modules for each component in the vehicle assembly (e.g., clutch, gearbox, wheel, differential, and others), which account for the combined effects of all sub-systems together. An overview of the model is shown in Figure 4.

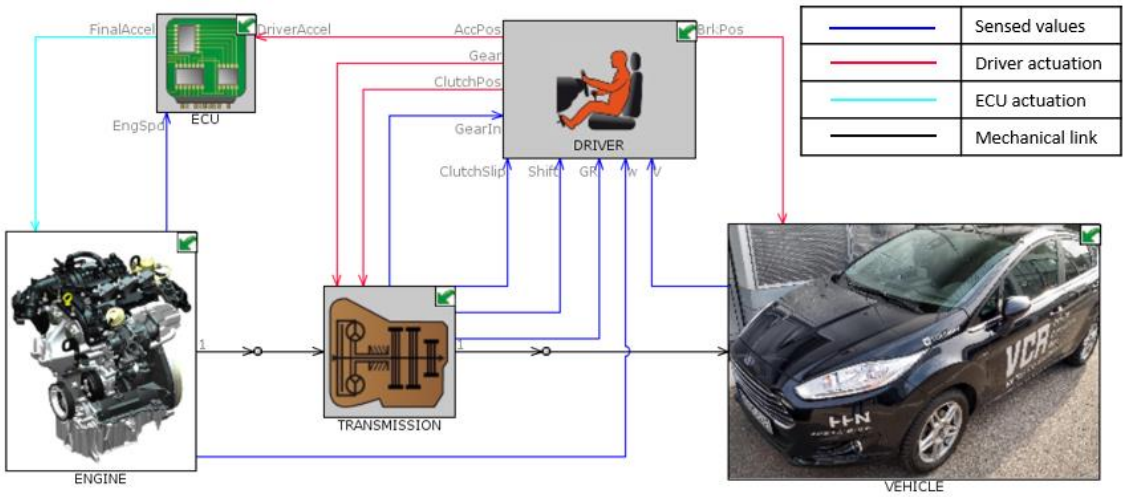

Figure 4 - GT-Suite vehicle model.

The Driver is the main component of the model, which is simulated as a controller that attempts to follow the desired vehicle speed profile with time. It initially actuates on the accelerator and brake pedals up to the point where the desired speed for gear shift (which is an optimizable parameter, as discussed and illustrated later) is achieved, then the clutch pedal is actuated, and gears are shifted. The vehicle accounts for the resistive power imposed by the road and environment to follow the desired curve. The transmission subsystem is responsible for the dynamic link between the engine and the vehicle differential. The proposed ECU conditions the input acceleration demand for idling and fuel cut conditions outputting and effective pedal demand to the engine. The map-based engine accounts for fuel consumption and emissions based on the imposed power demand.

3.2. Driving cycles

Nowadays, the homologation procedures carried out to evaluate the CO_2 and pollutant emissions from vehicles are achieving more rigorous levels. In the EU, the worldwide harmonized light vehicles test cycle (WLTC) arose to increase the transient load demand during the test procedures. The WLTC encompasses a more significant area of the engine operating map, to closely approach the real-world fuel consumption and emissions compared to the NEDC [48]. Dynamometer measurements made with 20 different light-duty passenger vehicles presented WLTC CO_2 emissions of up to 12% higher than those of NEDC [49]. In downsized engines, the explored range of operation is further increased in both driving cycles, providing a more thorough evaluation of the VCR system benefits and the penalties of the transition times. For reasons of brevity, the speed profiles and fundamental properties of the studied driving cycles are presented in Appendix A. Figure A.1 presents the WLTC driving cycle speed profile.

Since the purpose of the VCR system is to reduce the fuel consumption in the low/mid-load region of the engine map while maintaining operable conditions in the high load region, less load demanding cycles, such as urban cycles or urban sections of standard cycles, were selected to perform the study. In particular, three different urban cycles were proposed to evaluate this aspect [50]:

- ARTEMIS - Urban

- New York City Cycle
- TRAMAQ UG214 Car 08

The urban ARTEMIS driving cycle was developed from an extensive database (with 77 passenger cars) describing numerous European driving conditions and behaviors [51]. It accounts for almost any conditions found in urban traffic. The New York City Cycle was originally developed by the New York City Department of Environmental Protection to represent highly congested urban traffic conditions. TRAMAQ UG214 Car 08 was also used as a representative of congested urban traffic [52]. As a matter of reference, the ECE elementary urban cycle, which is a section of the NEDC, was also used in this study. The time-speed profiles of the four cycles are shown in Figure A.2. The WLTC – low (urban section of the WLTC) was used as a reference case for the urban driving cycles, providing long idling periods and steep load requirements with an expected large number of CR shifts.

Another parameter considered for the VCR system evaluation was the dynamic behavior of the driving cycle. This characteristic is relevant because abrupt load transitions (present in some urban cycles) cause the low CR to be activated more frequently and for a short period of time, leading to reduce the VCR system benefits. Highway cycles or sections of standard highway cycles possess steady high-speed conditions that enable the reduction of gear shifts number and smoother load transitions. In this scenario, mid to high loads with smoother transitions enable the average operating point at the best engine efficiencies. For this reason, two additional cycles were used to evaluate the VCR system:

- ARTEMIS – Motorway
- US06 – Highway

The ARTEMIS – Motorway accounts for the real highway conditions of steady and unsteady high-speed. The US06 driving cycle was created to expand the EPA FTP-75 to include engine conditions not covered during the test procedure [52]. In the present work, only the highway section of the US06 driving cycle, which takes place between the 131 and the 495 second of the speed profile, was evaluated, since the other two sections presented city (unsteady low speed) conditions. The speed profiles for these two driving cycles are shown in Figure A.3, while the main properties of all the studied driving cycles are presented in Table A.1. The WLTC – Extra-high (Freeway section of the WLTC) was applied as the reference case for the highway driving cycles, providing the evaluation of the reduced number of CR shifts due to the steadier speed profile associated to higher load conditions.

3.3. Transient VCR sub-model and VCR controller

The most straightforward control methodology for a two-stage VCR system is made by using a BMEP-engine speed switching curve [53]. In real applications, a hysteresis band is imposed on this kind of methodology to reduce the number of unnecessary CR shifts. In this study, a switching band was implemented for the transient VCR system, as presented in Figure 3(c). The bottom of the switching band is located at the frontier between gains and losses of the higher CR use due to the effort to reduce the use of the lower CR at any time bellow this frontier. Therefore, the switch from low to high CR occurs when the BMEP is below the frontier line. Whereas the opposite switch, from

high to low CR, occurs when BMEP is 0.05 MPa above the frontier line. The value of 0.05 MPa for switching bandwidth was selected since it was verified not to cause losses on the impact of the transient CR switching behavior on fuel consumption. This means that, if the bandwidth value is too large, the number of CR shifts is going to be massively reduced, losing information on the effects of CR transition. In the instantaneous switching VCR system, the CR shift occurs bi-directionally from the frontier line, also called herein optimum switch line.

Some studies have already presented the benefits of the VCR systems through driving cycles simulation [38,41]. Most of these studies use single maps containing both CRs, which means that the VCR mechanism is assumed to perform the CR switching instantaneously. However, this behavior is not compatible with real VCR mechanisms. In the present research, the effect of considering a realistic CR switching time is studied. For this purpose, a transient function for the used mechanism was determined.

The basic idea of using an isolated transient function for the CR switching is to evaluate the specific penalization caused by a slow transition from high to low CR, or vice-versa, in a driving cycle, thus enabling the optimization of the CR switching methodology. A scheme of the proposed sub-model is presented in Figure 5. The engine sub-assembly is shown on the bottom right side of the figure, with the corresponding links to the main model assembly (as shown in Figure 4). The VCR system represents the proposed model where the input to the model is the engine operating point (speed and BMEP), and the outputs are the instantaneous gains/losses in terms of consumption and emissions.

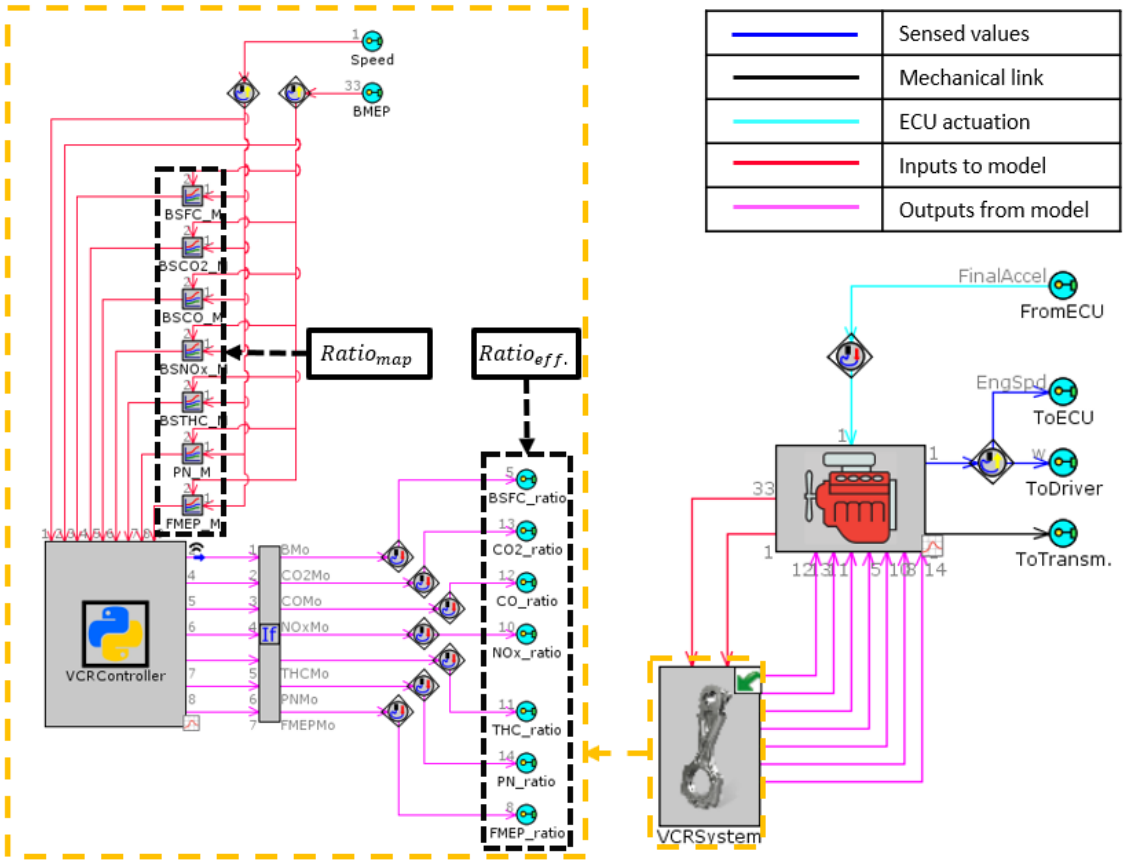

Figure 5 - Engine and VCR sub-assembly in GT-suite.

The components named $\mathrm{Ratio_{map}}$ are the looked-up ratios between high CR values and low CR values, e.g., the $\mathrm{BSFC_{ratio,map}}$ would be equivalent to $\mathrm{BSFC_{High\ CR}/BSFC_{Low\ CR}}$. The $\mathrm{Ratio_{eff}}$ are the outputs to the engine, which corresponds to the effective values of gains/losses based on the actual CR state and operating condition, i.e., based on the transition time from one CR to the other. The effective ratios were calculated as follows (considering de BSFC):

$$\mathrm{BSFC_{ratio,eff.}} = (\mathrm{BSFC_{ratio,map}x}) + (1 - \mathrm{x}) \quad (1)$$

Here, $BSFC_{ratio,map}$ is the looked-up values based on the operating condition. The variable x represents the actual compression ratio and is calculated by:

$$\mathrm{x} = \frac{\mathrm{t}-\mathrm{t_i}}{\Delta \mathrm{t}} \quad (2)$$

Where t is the actual simulation time, t_i is the time when the CR switch was demanded by the controller, and Δt is a polynomial function of the engine speed and BMEP, which represents the time needed for the transition to be completed. The transition times were based on the results presented in [45] and were separately accounted for low/high to high/low CR transitions. As the operating condition changes, the value of Δt also changes, thus promoting an acceleration or deceleration of the CR switch. More details on this function are presented in the following section.

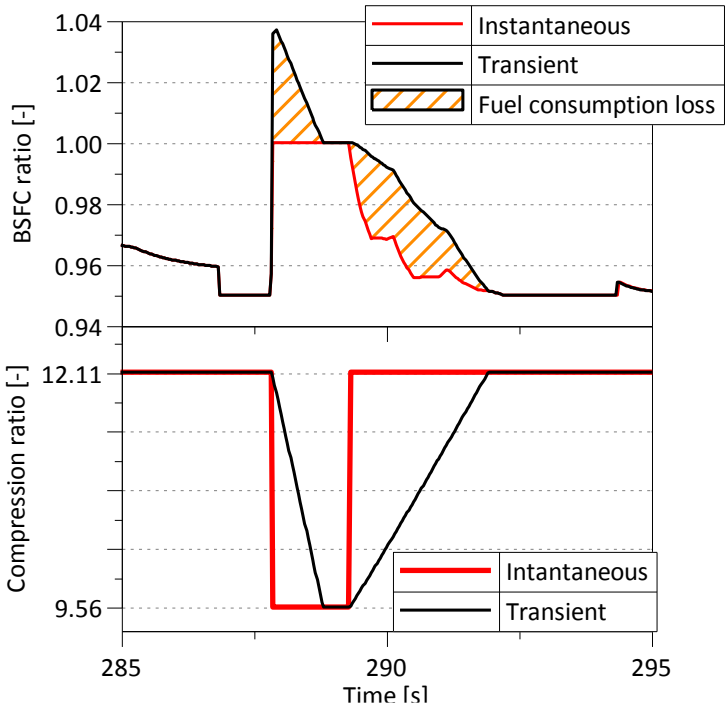

Figure 6 - Transient behavior of BSFC ratio (upper) and CR (bottom).

The resultant $\mathrm{Ratio_{eff.}}$ values were entered as gains to the low CR engine maps, which for values below/above one would result in a reduction/increase of the considered parameter. Figure 6 presents the transient behavior achievable with the VCR sub-model. Therefore, the isolated penalty of the slow transition behavior (in some conditions) could be instantaneously obtained and integrated into the cumulative results.

3.4. Switching time function

A switching time function was derived from the experimental data presented in [45]. A polynomial function was fitted as a function of the engine speed and BMEP, employing the least-squares method. The results of this function are presented in Figure 7 separately for the high to low CR transition event and vice-versa. The function represents the experimental data with an R-squared coefficient of more than 98%. It is observed that, in both transitions, the increase in engine speed reduces the time necessary for the CR switch. Nonetheless, as the engine load increases, the cylinder gas force increases, benefiting the high to low CR transition (which is a necessary safety measure against knock during highly step load increases) and hindering the opposite transition (which may cause penalties in terms of fuel consumption).

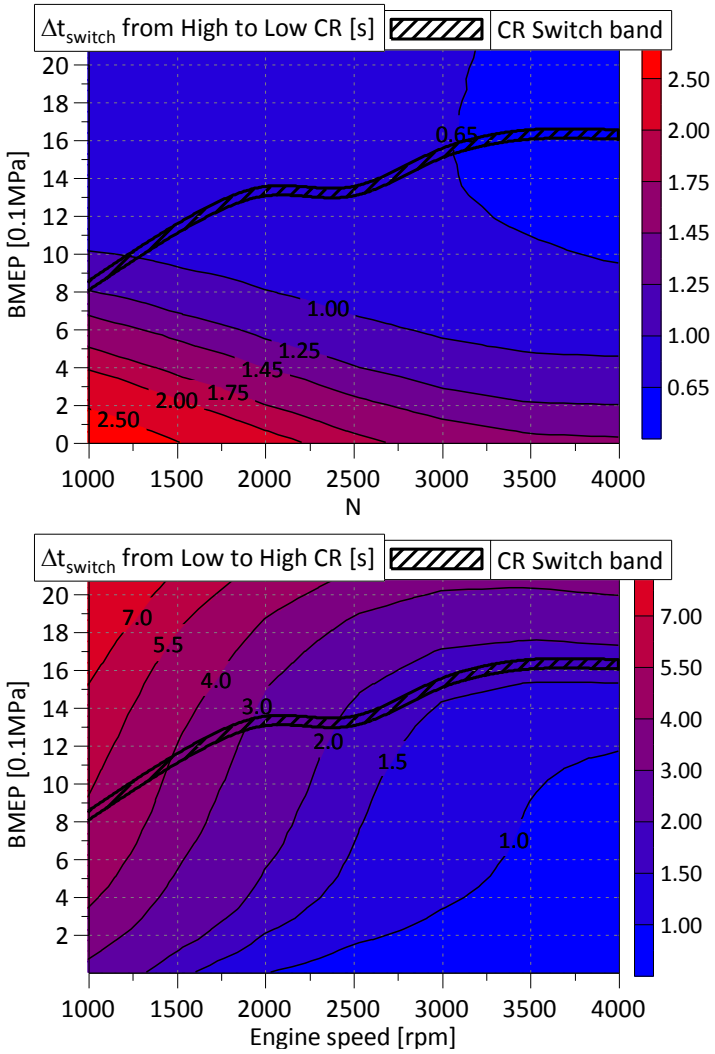

Figure 7 – CR switching transition duration.

The function was applied to the model presented in section 3.3, considering that, during the transition, the time needed to change the CR is variable, e.g., as the engine speed increases during a transition, the transition is accelerated.

4. Results and discussion

The results are divided into three subsections. In the first subsection, a detailed comparison between the VCR system and the fixed CR system was made for urban standard driving cycles. In the second subsection, the same comparison was performed for highway standard driving cycles. In the final subsection, the overall results of the fuel consumption benefits of the VCR system were presented.

4.1. VCR performance at urban cycles

To reduce the fuel consumption at low/mid-load, the application of VCR systems is highly valuable for urban traffic conditions. At long idling periods, the increased compression ratio would have the highest benefits because spark advance for maximum brake torque (MBT) conditions are always made possible. Thus, reducing the drawbacks of lower CR needed for downsized engines. The results presented herein are based on the already mentioned standard driving cycles (section 3.2) and vehicle (section 3.1), such that the load demand did not change for the three different proposed systems. Therefore, comparable results between Instantaneous switching VCR, Transient switching VCR, and Fixed CR could be analyzed with isolated effects for each one. Considering the steep load increase, possible with map-based simulations, the maximum fuel consumption penalties would appear (Figure 6). Therefore, the present results would have had the worse conditions to have long CR switching transitions.

The main parameter to be optimized on the proposed framework was the engine speed for gear up-shift. It was studied ranging from 1800 to 3800 rpm and kept constant for all the gears. Regarding the gear down-shift speed, it was taken at 500 rpm bellow the gear up-shift speed. Figure 8 presents the relative cycle time spent on each gear and the total number of gear shifts. The number of gear shifts within the cycle is a very discontinuous function of the gear up-shift speed due to the nature of the gear shift requirement itself. Therefore, scattered results for variables like fuel consumption and others were already expected.

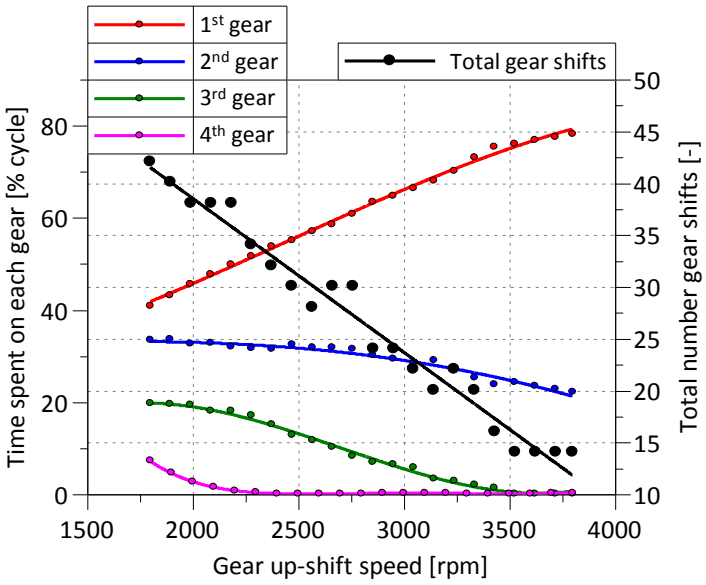

Figure 8 – WLTC (low): Percentage of cycle time spent on each gear (left) and the total number of gear shifts (right).

In urban driving cycles, lower vehicle speeds with highly dynamic load transitions are demanded. Thus, reducing the engine operating speed is a valuable resource for downsized engines in terms of fuel consumption reduction, as shown in Figure 9(a), as a result of the increased engine load operation and reduced pumping losses (made possible by the use of higher gear numbers). However, at low engine speed conditions, the time available for auto-ignition to occur increases [54], and the benefits of high CR use are limited. Figure 9(b) depicts the improvement of relative fuel consumption for the VCR systems with respect to fixed CR ones. As the engine speed for gear up-shifting increases, the average engine load and, consequently, the range of engine load operation is reduced, increasing the time spent on high CR (Figure 9(c)) with the VCR system. This feature allows extending the use of regions of the map with higher consumption benefit, as shown in Figure 10, which presents the instantaneous operation points and their corresponding CR for two different gear up-shift speeds. Despite the improved relative fuel consumption benefits at higher gear up-shift speed, in absolute terms, the best up-shift speed has not changed much with respect to the fixed CR case.

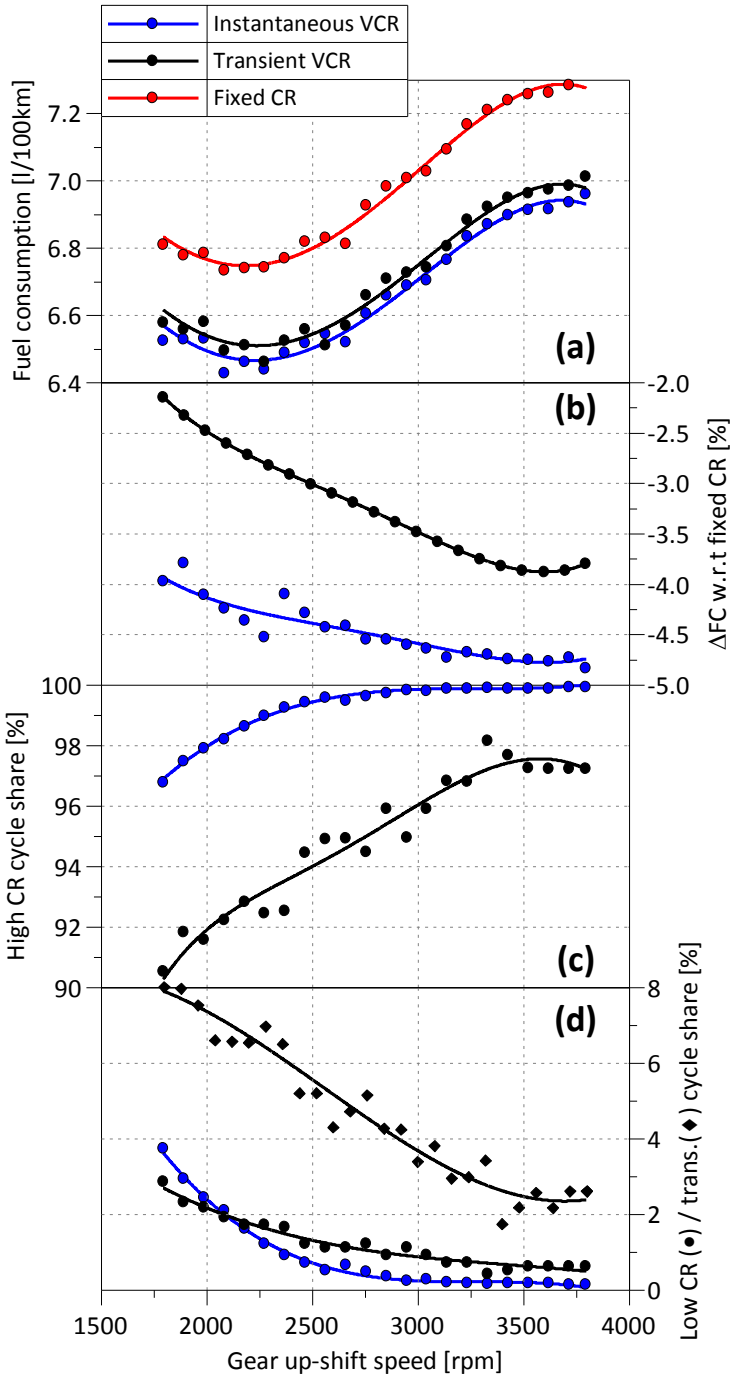

Figure 9 - WLTC (low): Gear up-shift speed parametric study results. (a): Average cycle fuel consumption; (b): Fuel consumption difference with respect to Fixed CR; (c): Percentage of cycle time spent on high CR; (d): Percentage of cycle time spent on low CR and transitions.

Considering the functions presented in Figure 7 (used in the transient VCR system), the low-speed efficiency gains are further obstructed by the high amount of time spent in transitions (Figure 9(d)). As it is confirmed in Figure 10, the predominant fraction of time spent on transitions is associated to the shift from low to high CR. This result is a particular drawback of the mechanism design, which enables a faster transition from high to low CR for safety reasons. This fact leads to a fuel consumption reduction of only 2%, compared to the 4% achievable with the instantaneous switching operation (in the worst-case scenario), as shown on the left side of Figure 9(b).

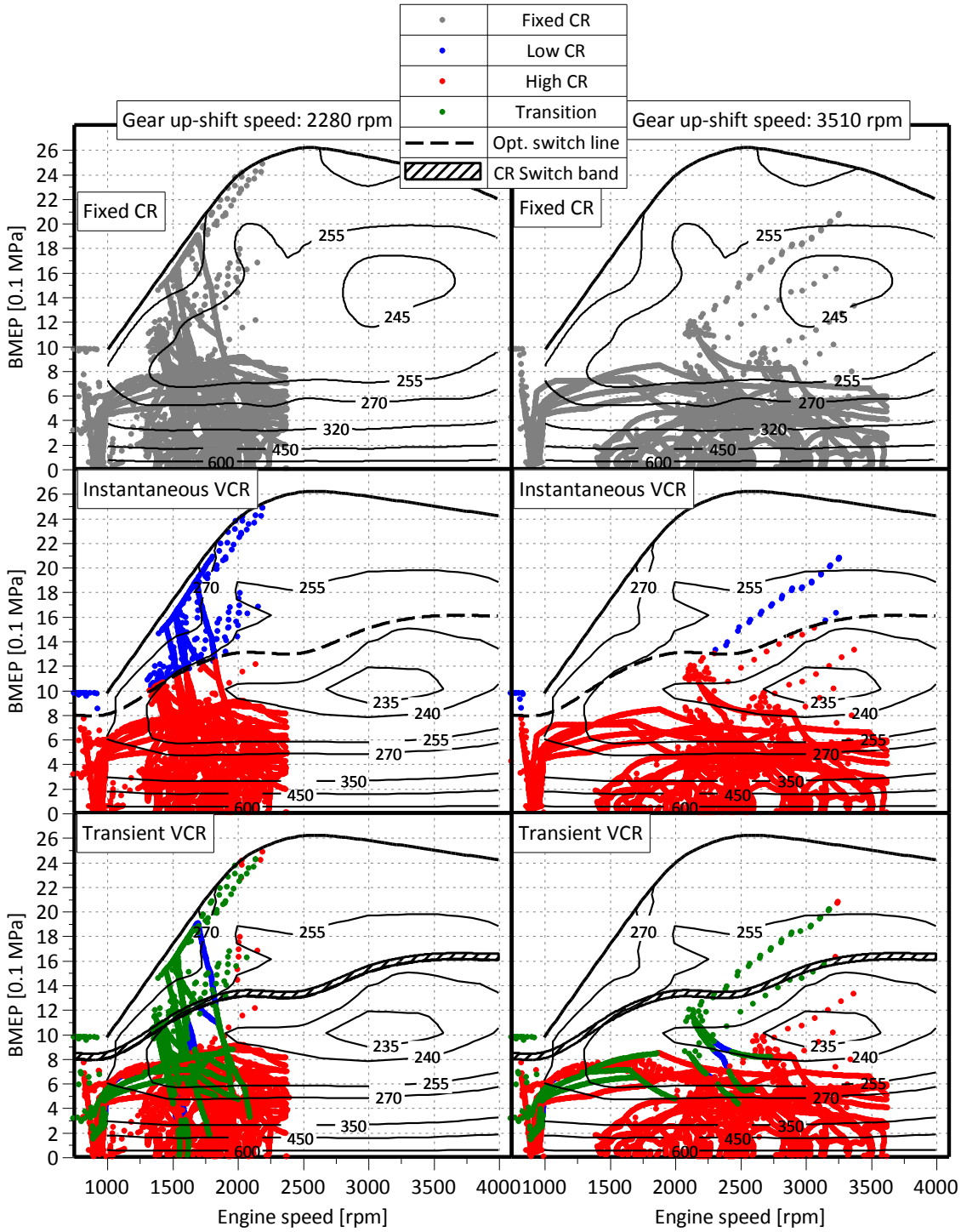

Figure 10 – WLTC (low): operating points and corresponding CR in the fixed CR and VCR BSFC maps.

A summary of the trends for relative fuel consumption differences is shown in Figure 11 for all the simulated urban driving cycles. Despite the differences due to the variety of conditions proposed for each different cycle, the trends clearly show the highest relative reductions of fuel consumption at increased engine speeds for gear up-shift due to the reduce average load operation. The resultant levels of relative fuel consumption benefit are straightforwardly related to the cycle average positive acceleration, shown in Table A.1, of each driving cycle. Hence, higher average positive acceleration values could be related to the higher dynamic demand of the cycle. This favors the increased

number of CR switches and the time spent on low CR, thus reducing the benefits of the VCR system.

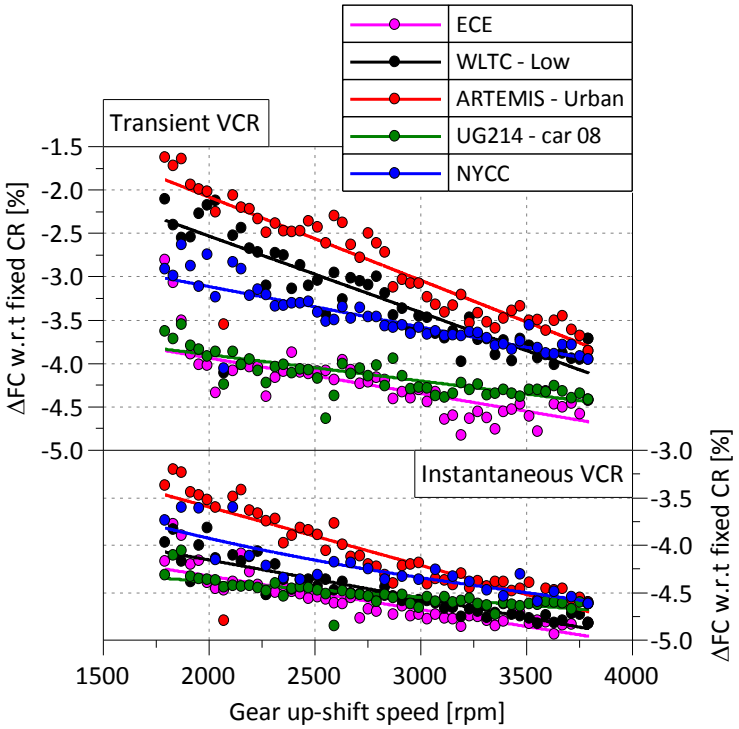

Figure 11 - Urban driving cycles relative fuel consumption difference w.r.t. fixed CR.

The highest reduction of relative fuel consumption can be seen for lower dynamic cycles, such as the ECE, which is known as a synthetic profile cycle. This effect was attributed to the lower time spent on transitions or low CR, achieving values closer to the instantaneous switching VCR. This behavior could also be seen for the TRAMAQ UG214 – car 08. Regardless of its congested traffic conditions, the dynamic behavior was not so high as to strongly affect the transient VCR system. Oppositely, the effects of transition times were more visible on the more aggressive cycles, further differentiating the transient VCR system from the instantaneous one. This effect was mainly seen in the ARTEMIS – urban cycle, which covers a higher amount of urban traffic conditions. Whereas, in the NYCC, higher vehicle accelerations are reached at each vehicle launch. Therefore, conditions for CR switch were reached throughout the entire cycle.

4.2. VCR performance at highway cycles

The same analysis performed in the previous section was made for the highway driving cycles. In highway cycles, such as the presented WLTC extra-high, the vehicle speed is taken to extreme conditions, while the load transitions are not so dynamic. Thereby, as presented in Figure 12, the relative number of gear shifts is remarkably reduced compared to the urban cycle, and higher gear numbers are dominant throughout the cycle. As the gear up-shift speed is increased, the engine load demand is reduced by the use of smaller gear numbers (higher gear ratios), which is a factor in favor of the VCR system.

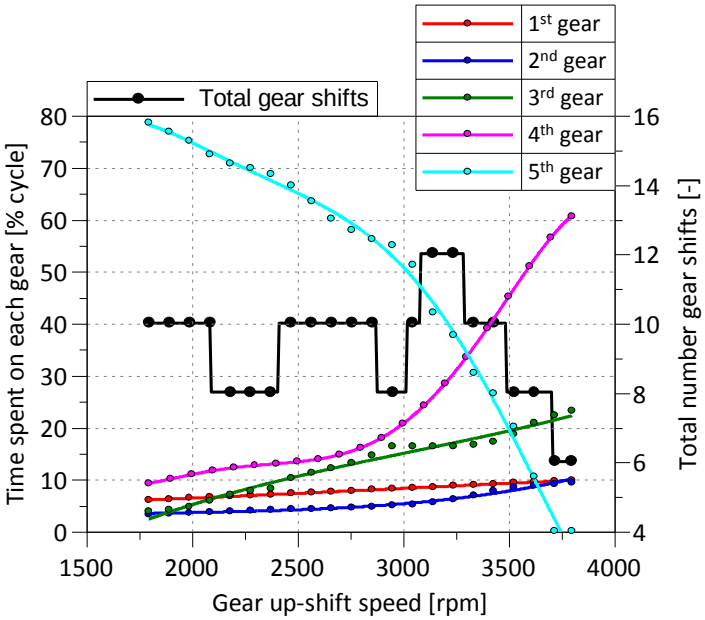

Figure 12 - WLTC (extra-high): Percentage of cycle time spent on each gear (left) and the total number of gear shifts (right).

Figure 13 shows the results of the performed parametric study. The trends presented in Figure 13(a) can be mainly related to the cycle contributions of the 4th and 5th gears (Figure 12). For the proposed powertrain, the high speed demanded by the cycle reaches 3000 rpm in the 5th gear regardless of the gear up-shift speed (Figure 14 (left)). Therefore, high fuel consumption reductions can be seen for the lowest gear up-shift speed for the instantaneous VCR system. This effect appeared because the 5th gear was reached very fast, maintaining higher load operating points (with low fuel consumption) for a longer time without the drawbacks of high CR transition durations.

With the increase in the gear up-shift speed, up to the point that it reaches around 3000 rpm, the relative fuel consumption increases. In this region, the 5th gear takes longer to be reached, and an inferior relative fuel consumption region was explored. After a gear up-shift speed of 3000 rpm, the percentage of the 4th and 5th gears have an abrupt slope change, which promotes a progressive reduction of the engine load requirement. Hence, the fixed CR is evenly penalized by part-load inefficiencies, while VCR systems are relatively benefited. After this point, the minimum/maximum time spent on low/high CR has been reached (Figure 13(c) and (d)), thus explaining the progressive reduction of relative fuel consumption.

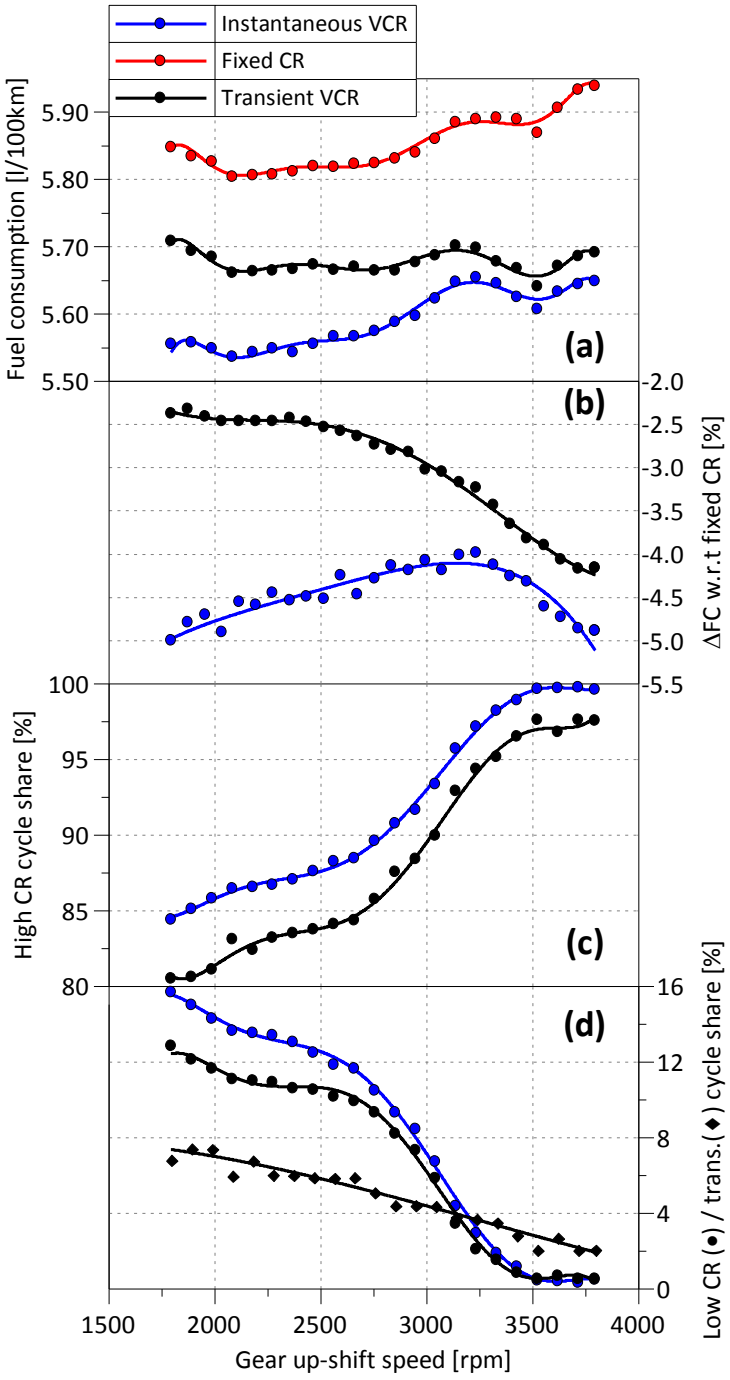

Figure 13 - WLTC (extra-high): Gear up-shift speed parametric study results. (a): Average cycle fuel consumption; (b): Fuel consumption difference with respect to Fixed CR; (c): Percentage of cycle time spent on high CR; (d): Percentage of cycle time spent on low CR

Up to 2500 rpm of gear up-shift speed, the relative gains of the transient VCR fuel consumption are constantly limited by higher CR transition durations. As can be seen in Figure 14 (left), the CR transition state occupies a considerable percentage of the high load conditions (above the CR switching frontier) and part-load (slightly below the switching line), leading to behaviors such as the ones presented in Figure 6. After this up-shifting speed, the trend gets closer to the one presented for urban driving cycles (Figure 11). The average load demand decreases and the low CR share of the cycle reach its minimum values. The effects overlap occurring for the transient VCR system, either

before or after the gear up-shift speed of 2500 rpm, produce an almost constant consumption, being considered independent from this parameter at these driving cycle conditions, thus resulting in a reduction of the driver style dependency.

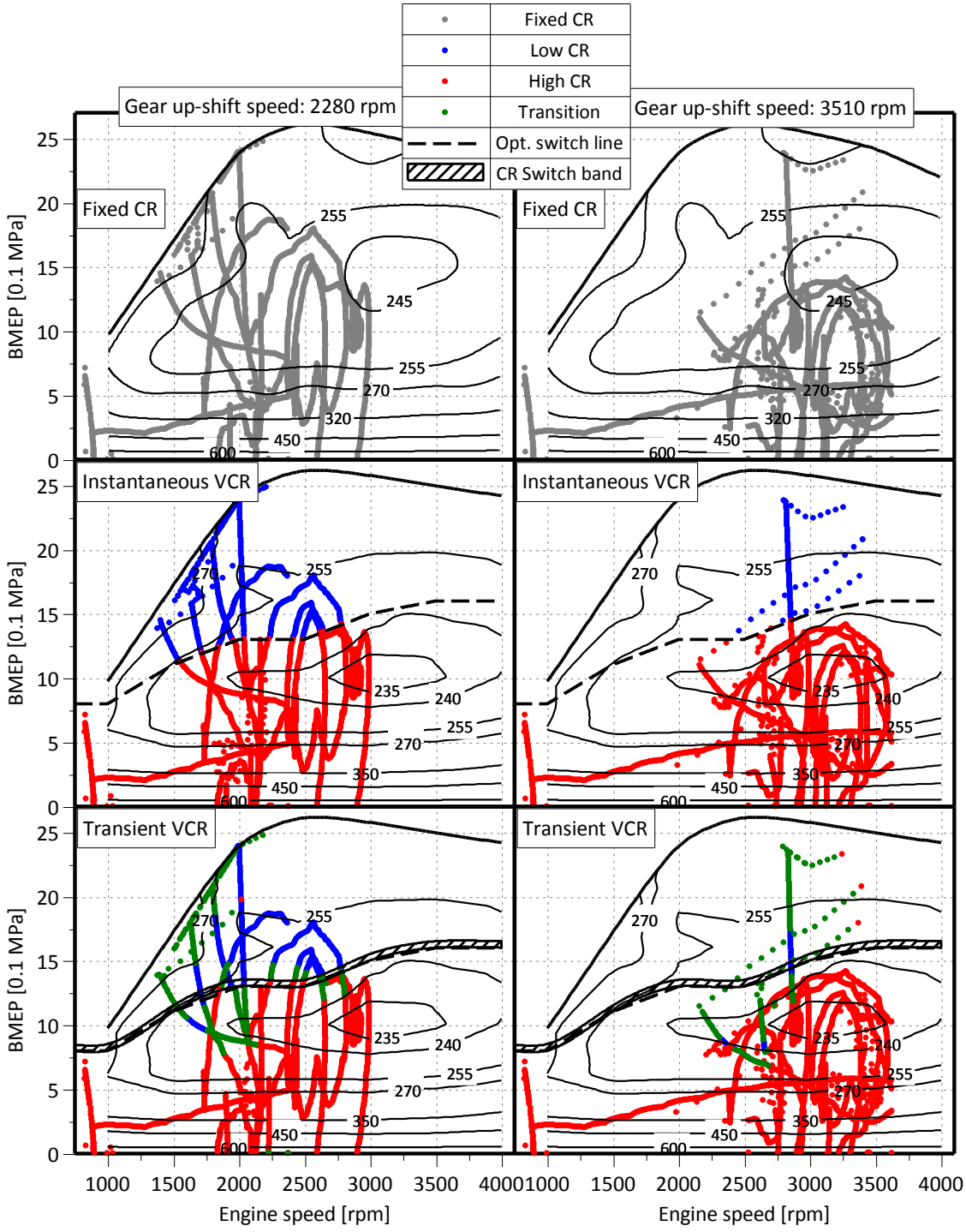

Figure 14 - WLTC (extra-high): operating conditions and CR in the BSFC maps.

The same trends presented for the WLTC are also seen for the other two highway driving cycles (Figure 15), changing only the specific gear up-shift speed where the minimum relative fuel consumption benefit is reached (inflection point for the instantaneous VCR system). This feature is mainly related to the properties of the driving cycle itself, such as maximum speed, as presented in subsection 3.2 and appendix A.

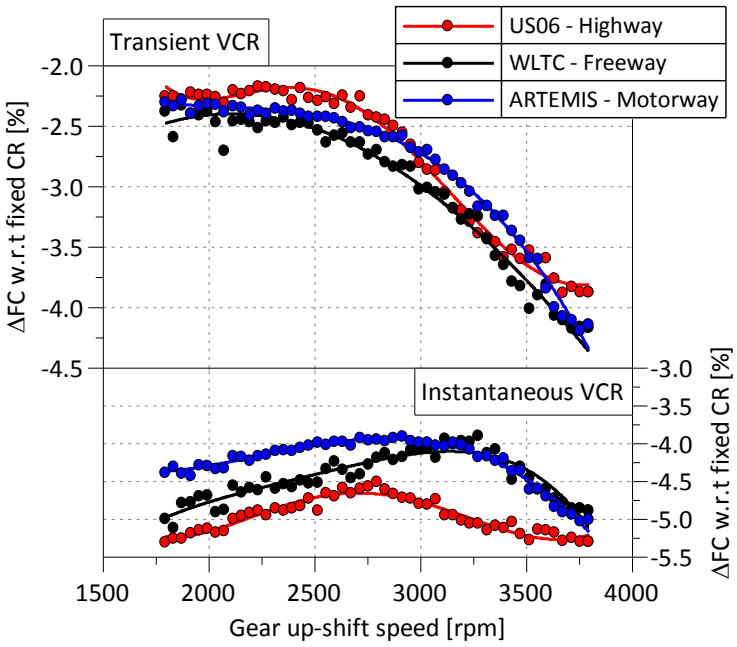

Figure 15 - Highway driving cycles relative fuel consumption difference w.r.t. fixed CR.

The constant relative fuel consumption gains within smaller gear up-shift region, and also the increasing benefits after 2500 rpm are presented at the same levels as in the WLTC for the transient VCR system. This effect suggests that the relative gain is not predominantly linked to the dynamic behavior of the cycle but to the transition duration itself (Figure 7). However, some higher relative benefits could be seen in the instantaneous VCR system. In the case of the US06 – highway cycle, high-speed conditions encompassed a more significant quantity of the cycle, maintaining the engine at higher load levels with enlarged CR transition durations.

4.3. General VCR benefit trends

As a summary of the main results, a comparison of the benefits of the VCR system at the different driving conditions analyzed is presented in Figure 16. There, the optimum gear up-shift speed of each system on each driving cycle is compared to obtain an overall evaluation of the VCR system concerning the fixed CR system. The absolute fuel consumption, presented on the bottom of Figure 16, presents a strong correlation with the driving cycles itself. In the urban driving cycle cases, a strong correlation between fuel consumption and the average vehicle speed (Table A.1) can be seen. As also presented in [55], this trend appears for low-speed driving cycles as a result of the smaller efficiency when operated with lower vehicle speeds. This effect is caused by an increase in the use of lower gear numbers reducing the demanded BMEP, and thus, the operated BSFC.

As shown in Figure 16, the absolute results for highway driving cycles did not change much between each other. The most visible result is the reduction of the transient VCR benefits in the US – highway, mainly attributed due to its higher averaged operating BMEP due to a slightly higher average speed. Therefore, increasing the transition durations and the time spent on low CR.

A reduction of up to 5% in fuel consumption could be reached on the proposed conditions with the ideal instantaneous switching VCR system. Nonetheless, the average reduction was around 4% for most of the studied cases. Because of the non-instantaneous switching, fuel consumption penalties of around 1% for most urban cycles and 2% for highway cycles concerning the instantaneous system are obtained.

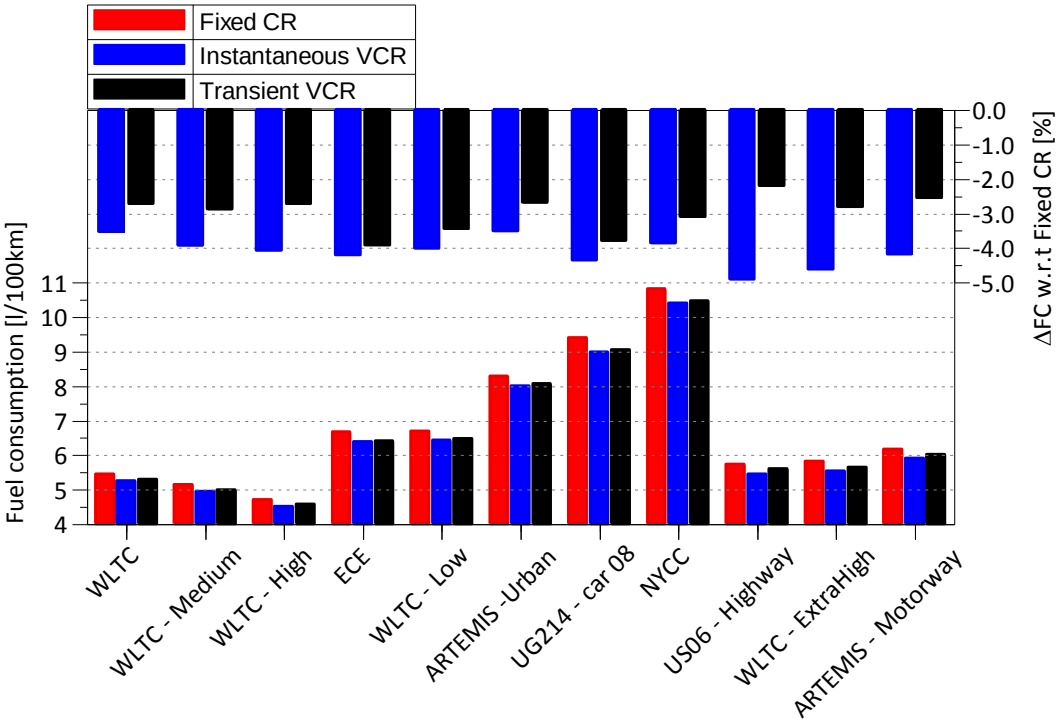

Figure 16 - Fuel consumption and relative FC difference for all proposed cycles at optimum conditions (up-shift speed for minimum FC) for each system.

Finally, it can be said that the transient switching system evaluation provided more reliable results for the evaluation, optimization, and development of variable length connecting rod VCR engines.

5. Conclusions

The present work investigated the potential of a VCR system application to a state-of-the-art downsized SI engine used in a compact passenger car commercially available in Europe and the United States. The transition times between the two compression ratios were used as input information in a driving cycle simulation model to account for the fuel consumption penalties during the real VCR operation with respect to an instantaneous system. The following conclusions can be extracted from this study:

- The simple map-based model was found to be a good starting point to evaluate the isolated losses accounted for non-ideal VCR systems since the operating points were the same for all the proposed systems.

- The low-end torque region of the engine operating map was shown to be the most limiting part for VCR benefiting, mainly because of the highly increased transition times from high to low CR. Furthermore, higher knock probability is present in this region, excessively reducing the high CR benefits.

- As the torque demand was reduced through higher engine speed operation, the relative benefits of the VCR application were highly increased by the enlarged time spent on high CR at all simulated driving cycles.

- Despite the higher fuel consumption benefits with the instantaneous VCR system at highway driving cycles, the higher transition durations at such load conditions left the highest benefits (with the transient VCR system) to the urban driving cycles.

- Considering that no recalibration was performed (in terms of injection timing and pressure, intake and exhaust valve timings, and oil pressure) for the original ones, favorable results of up to 4% of average fuel consumption reductions could be achieved by the transient (i.e., real) VCR system.

Future work – The sub-model presented in this study to account for the transient penalties of a two-stage VCR system can be further applied in studies of control strategy optimization or on parametric studies with other systems. The sub-model can also be applied in combination with the transition behavior of other engine systems, such as turbocharger response modeling, spark advance control, among others, to account for the whole system dynamics and results.

Acknowledgments

This research has been partially funded by FEDER and the Spanish Government through project RTI2018-102025-B-I00. The authors also acknowledge the Universitat Politècnica de València for partially supporting this research through Convocatoria de ayudas a Primeros Proyectos de Investigación (PAID-06-18).

Appendix A

This section presents more information related to the standard driving cycles presented in section 3.2.

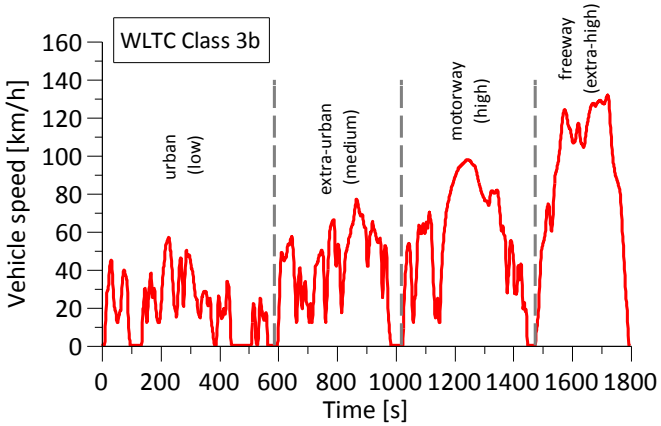

Figure A.1 - Worldwide harmonized light vehicles test cycle (WLTC) vehicle speed profile.

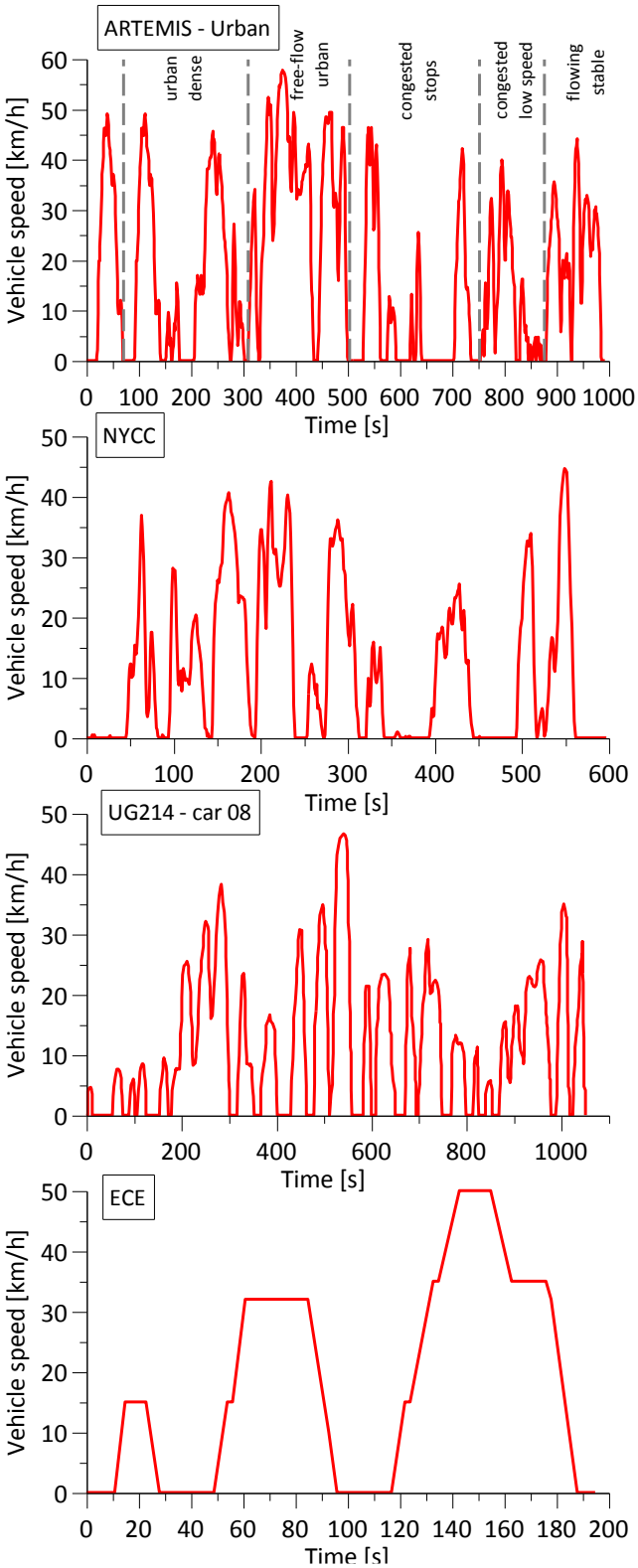

Figure A.2 - Urban driving cycles speed profiles (a): ARTEMIS – Urban, (b): New York City Cycle, (c): TRAMAQ UG214 – car 08, (d): ECE section of New European driving cycle.

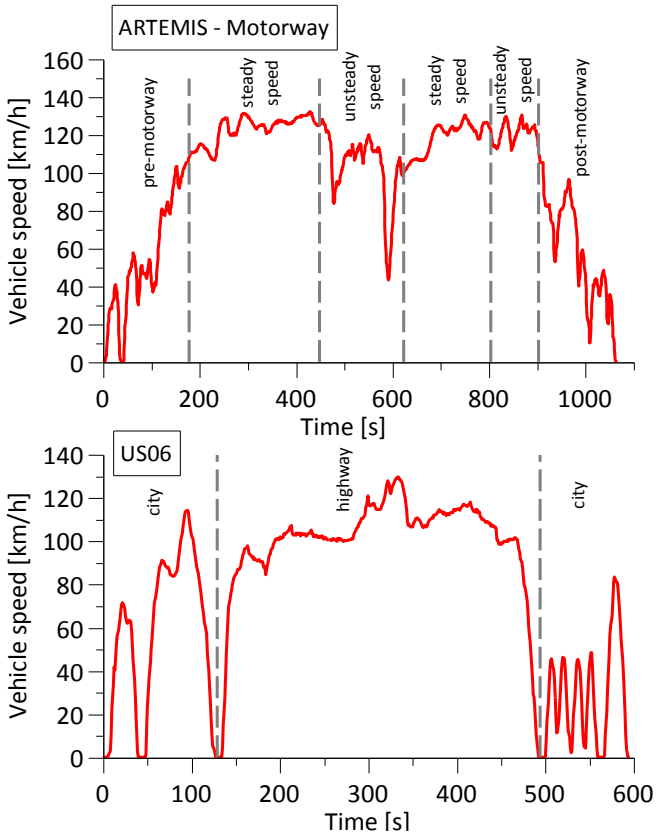

Figure A.3 - Highway driving cycles speed profiles (a): ARTEMIS – Motorway, (b): US06.

Table A.1 - Standard driving cycle main properties

Category	Driving cycle	Total time [s]	Average vehicle speed [km/h]	Maximum vehicle speed [km/h]	Average positive acceleration [m/s^2]	Distance [km]	Relative Positive Acceleration [m/s^2]
Reference	WLTC Class 3b	1800	46.5	131.3	0.497	23.266	0.148
	WLTC – Medium 3	433	39.2	76.6	0.530	4.76	0.190
	WLTC – High 3	455	56.7	97.4	0.501	7.16	0.122
Urban	ECE	195	18.4	50.1	0.348	0.995	0.147
	WLTC - Low 3	589	18.9	56.5	0.483	3.095	0.205
	ARTEMIS – Urban	993	17.7	57.3	0.531	4.874	0.272
	UG214 – car 08	1057	12.5	47.4	0.337	3.658	0.185
	NYCC	598	11.5	44.5	0.466	1.903	0.250
Highway	US06 - Highway	364	97.1	128.9	0.306	10.035	0.113
	WLTC – Extra-high	323	92.0	131.3	0.299	8.254	0.125
	ARTEMIS – Motorway	1068	96.9	131.4	0.273	28.737	0.115

References

[1] Amelang S, Wehrmann B. Dieselgate - a timeline of Germany's car emissions fraud scandal | Clean Energy Wire n.d. https://www.cleanenergywire.org/factsheets/dieselgate-timeline-germanys-car-emissions-fraud-scandal (accessed September 2, 2019).

[2] Luján JM, Bermúdez V, Dolz V, Monsalve-Serrano J. An assessment of the real-world driving gaseous emissions from a Euro 6 light-duty diesel vehicle using a portable emissions measurement system (PEMS). Atmos Environ 2018;174:112–21. doi:10.1016/j.atmosenv.2017.11.056.

[3] E J, Pham M, Zhao D, Deng Y, Le DH, Zuo W, et al. Effect of different technologies on combustion and emissions of the diesel engine fueled with biodiesel: A review. Renew Sustain Energy Rev 2017;80:620–47. doi:10.1016/j.rser.2017.05.250.

[4] Jurić F, Petranović Z, Vujanović M, Katrašnik T, Vihar R, Wang X, et al. Experimental and numerical investigation of injection timing and rail pressure impact on combustion characteristics of a diesel engine. Energy Convers Manag 2019;185:730–9. doi:10.1016/j.enconman.2019.02.039.

[5] E J, Zhao X, Qiu L, Wei K, Zhang Z, Deng Y, et al. Experimental investigation on performance and economy characteristics of a diesel engine with variable nozzle turbocharger and its application in urban bus. Energy Convers Manag 2019;193:149–61. doi:10.1016/j.enconman.2019.04.062.

[6] Jiaqiang E, Zuo W, Gao J, Peng Q, Zhang Z, Hieu PM. Effect analysis on pressure drop of the continuous regeneration-diesel particulate filter based on NO2 assisted regeneration. Appl Therm Eng 2016;100:356–66. doi:10.1016/j.applthermaleng.2016.02.031.

[7] Huang Y, Ng ECY, Yam Y shing, Lee CKC, Surawski NC, Mok W chuen, et al. Impact of potential engine malfunctions on fuel consumption and gaseous emissions of a Euro VI diesel truck. Energy Convers Manag 2019;184:521–9. doi:10.1016/j.enconman.2019.01.076.

[8] Deng Y, Liu H, Zhao X, Jiaqiang E, Chen J. Effects of cold start control strategy on cold start performance of the diesel engine based on a comprehensive preheat diesel engine model. Appl Energy 2018;210:279–87. doi:10.1016/j.apenergy.2017.10.093.

[9] García A, Monsalve-Serrano J, Heuser B, Jakob M, Kremer F, Pischinger S. Influence of fuel properties on fundamental spray characteristics and soot emissions using different tailor-made fuels from biomass. Energy Convers Manag 2016;108:243–54. doi:10.1016/j.enconman.2015.11.010.

[10] Benajes J, Pastor J V., García A, Boronat V. A RCCI operational limits assessment in a medium duty compression ignition engine using an adapted compression ratio. Energy Convers Manag 2016;126:497–508. doi:10.1016/j.enconman.2016.08.023.

[11] Benajes J, García A, Monsalve-Serrano J, Villalta D. Benefits of E85 versus gasoline

as low reactivity fuel for an automotive diesel engine operating in reactivity controlled compression ignition combustion mode. Energy Convers Manag 2018;159:85–95. doi:10.1016/j.enconman.2018.01.015.

[12] Wang Z, Liu H, Reitz RD. Knocking combustion in spark-ignition engines. Prog Energy Combust Sci 2017;61:78–112. doi:10.1016/j.pecs.2017.03.004.

[13] Santos H, Costa M. Evaluation of the conversion efficiency of ceramic and metallic three way catalytic converters. Energy Convers Manag 2008;49:291–300. doi:10.1016/j.enconman.2007.06.008.

[14] Heck RM, Farrauto RJ. Automobile exhaust catalysts. Appl Catal A Gen 2001;221:443–57. doi:10.1016/S0926-860X(01)00818-3.

[15] Feng D, Wei H, Pan M. Comparative study on combined effects of cooled EGR with intake boosting and variable compression ratios on combustion and emissions improvement in a SI engine. Appl Therm Eng 2018;131:192–200. doi:10.1016/j.applthermaleng.2017.11.110.

[16] European Environment Agency (EEA). Monitoring CO2 emissions from new passenger cars and vans in 2017. 2018. doi:10.2800/74986.

[17] Society of Motor Manufacturers and Traders (SMMT). Fall in new car market wake up call to policy makers as environmental goals at risk. 2019.

[18] Mock P. Emission Standards for Passenger Cars and Light-Commercial Vehicles in the European Union. ICCT Policy Updat 2019.

[19] Kalghatgi GT. Developments in internal combustion engines and implications for combustion science and future transport fuels. Proc Combust Inst 2015;35:101–15. doi:10.1016/j.proci.2014.10.002.

[20] Su J, Xu M, Li T, Gao Y, Wang J. Combined effects of cooled EGR and a higher geometric compression ratio on thermal efficiency improvement of a downsized boosted spark-ignition direct-injection engine. Energy Convers Manag 2014;78:65–73. doi:10.1016/j.enconman.2013.10.041.

[21] Zhen X, Wang Y, Xu S, Zhu Y, Tao C, Xu T, et al. The engine knock analysis - An overview. Appl Energy 2012;92:628–36. doi:10.1016/j.apenergy.2011.11.079.

[22] Heywood JB. Internal Combustion Engines Fundamentals. 2nd ed. McGraw-Hill Education; 2018.

[23] Zhuang Y, Qian Y, Hong G. The effect of ethanol direct injection on knock mitigation in a gasoline port injection engine. Fuel 2017;210:187–97. doi:10.1016/j.fuel.2017.08.060.

[24] Zhou L, Dong K, Hua J, Wei H, Chen R, Han Y. Effects of applying EGR with split injection strategy on combustion performance and knock resistance in a spark assisted compression ignition (SACI) engine. Appl Therm Eng 2018;145:98–109. doi:10.1016/j.applthermaleng.2018.09.001.

[25] Bozza F, De Bellis V, Teodosio L. Potentials of cooled EGR and water injection for knock resistance and fuel consumption improvements of gasoline engines. Appl

Energy 2016;169. doi:10.1016/j.apenergy.2016.01.129.

[26] Luján JM, Climent H, Novella R, Rivas-Perea ME. Influence of a low pressure EGR loop on a gasoline turbocharged direct injection engine. Appl Therm Eng 2015;89:432–43. doi:10.1016/j.applthermaleng.2015.06.039.

[27] Li T, Wang B, Zheng B. A comparison between Miller and five-stroke cycles for enabling deeply downsized, highly boosted, spark-ignition engines with ultra expansion. Energy Convers Manag 2016;123:140–52. doi:10.1016/j.enconman.2016.06.038.

[28] Lanzanova TDM, Dalla Nora M, Martins MES, Machado PRM, Pedrozo VB, Zhao H. The effects of residual gas trapping on part load performance and emissions of a spark ignition direct injection engine fuelled with wet ethanol. Appl Energy 2019;253:113508. doi:10.1016/j.apenergy.2019.113508.

[29] Noce T, da Silva RR, Morais R, Sales LCM, Hanriot S de M, Sodré JR. Energy factors for flexible fuel engines and vehicles operating with gasoline-ethanol blends. Transp Res Part D Transp Environ 2018;65:368–74. doi:10.1016/j.trd.2018.09.002.

[30] Asthana S, Bansal S, Jaggi S, Kumar N. A Comparative Study of Recent Advancements in the Field of Variable Compression Ratio Engine Technology. SAE Tech Pap 2016-01-0669 2016;1. doi:10.4271/2016-01-0669.

[31] Wittek K, Geiger F, Andert J, Martins MES, Oliveira M. An Overview of VCR Technology and Its Effects on a Turbocharged DI Engine Fueled with Ethanol and Gasoline. SAE Tech Pap 2017:2017-36–0357. doi:10.4271/2017-36-0357.

[32] Hiyoshi R. Variable compression ratio engine. US2013/0327302A1, 2013.

[33] Moteki K, Fujimoto H, Aoyama S. Variable compression ratio mechanism of reciprocating internal combustion engine. US6505582B2, 2003.

[34] Larsen GJ. Reciprocating piston engine with a varying compression ratio. US5025757A, 1991.

[35] Wittek K. Hydraulic freewheel for an internal combustion engine with variable compression ratio. US9677469B2, 2017.

[36] Rao VDN, German DJ, Vrsek GA, Chottiner E, Madin MM. Variable compression ratio pistons and connecting rods. US6568357B1, 2003.

[37] Wittek K. Variables Verdichtungsverhältnis beim Verbrennungsmotor durch Ausnutzung der im Triebwerk wirksamen Kräfte. RWTH Aachen, 2006.

[38] Kleeberg H, Tomazic D, Dohmen J, Wittek K, Balazs A. Increasing Efficiency in Gasoline Powertrains with a Two-Stage Variable Compression Ratio (VCR) System. SAE Tech Pap 2013:2013-01–0288. doi:10.4271/2013-01-0288.

[39] Shelby MH, Leone TG, Byrd KD, Wong FK. Fuel Economy Potential of Variable Compression Ratio for Light Duty Vehicles. SAE Int J Engines 2017;10:2017-01–0639. doi:10.4271/2017-01-0639.

[40] Boretti A, Scalzo J. Novel Crankshaft Mechanism and Regenerative Braking System to Improve the Fuel Economy of Light Duty Vehicles and Passenger Cars. SAE Int J Passeng Cars - Mech Syst 2012;5:1177–93. doi:10.4271/2012-01-1755.

[41] Teodosio L, De Bellis V, Bozza F, Tufano D. Numerical Study of the Potential of a Variable Compression Ratio Concept Applied to a Downsized Turbocharged VVA Spark Ignition Engine. SAE Tech Pap 2017:2017-24–0015. doi:10.4271/2017-24-0015.

[42] Hoyer KS, Moore WR, Confer K. A Simulation Method to Guide DISI Engine Redesign for Increased Efficiency using Alcohol Fuel Blends. SAE Int J Engines 2010:2010-01–1203. doi:10.4271/2010-01-1203.

[43] Schmid A, Grill M, Berner H-J, Bargende M. Transient and Map-Based Driving Cycle Calculation with GT-SUITE. GT-User Conf., 2009.

[44] Luján JM, García A, Monsalve-Serrano J, Martínez-Boggio S. Effectiveness of hybrid powertrains to reduce the fuel consumption and NOx emissions of a Euro 6d-temp diesel engine under real-life driving conditions. Energy Convers Manag 2019;199:111987. doi:10.1016/j.enconman.2019.111987.

[45] Wittek K, Geiger F, Andert J, Martins M, Cogo V, Lanzanova T. Experimental investigation of a variable compression ratio system applied to a gasoline passenger car engine. Energy Convers Manag 2019;183:753–63. doi:10.1016/j.enconman.2019.01.037.

[46] Klein P. Zylinderdruckbasierte Fuellungserfassung für Verbrennungsmotoren 2009.

[47] Taylor JR. An introduction to error analysis. 2nd ed. 1997.

[48] Gao J, Chen H, Li Y, Chen J, Zhang Y, Dave K, et al. Fuel consumption and exhaust emissions of diesel vehicles in worldwide harmonized light vehicles test cycles and their sensitivities to eco-driving factors. Energy Convers Manag 2019;196:605–13. doi:10.1016/j.enconman.2019.06.038.

[49] Tsokolis D, Tsiakmakis S, Dimaratos A, Fontaras G, Pistikopoulos P, Ciuffo B, et al. Fuel consumption and CO 2 emissions of passenger cars over the New Worldwide Harmonized Test Protocol. Appl Energy 2016;179:1152–65. doi:10.1016/j.apenergy.2016.07.091.

[50] T. J. Barlow I. S. McCrae, and P. G. Boulter SL. A reference book of driving cycles for use in the measurement of road vehicle emissions. 2009.

[51] André M. The ARTEMIS European driving cycles for measuring car pollutant emissions. Sci Total Environ 2004;334–335:73–84. doi:10.1016/j.scitotenv.2004.04.070.

[52] Giakoumis EG. Driving and Engine Cycles. Springer; 2017. doi:10.1007/978-3-319-49034-2.

[53] Wittek K, Tiemann C, Pischinger S. Two-Stage Variable Compression Ratio with Eccentric Piston Pin and Exploitation of Crank Train Forces. SAE Int J Engines

2009;2:1304–13. doi:10.4271/2009-01-1457.

[54] Caton JA. The interactions between IC engine thermodynamics and knock. Energy Convers Manag 2017;143:162–72. doi:10.1016/j.enconman.2017.04.001.

[55] Berry I. The Effects of Driving Style and Vehicle Performance on the Real-World Fuel Consumption of U.S. Light-Duty Vehicles. Virginia Polytechnic Institute and State University, 2007.

Abbreviations

BMEP	Brake mean effective pressure	ICE	Internal combustion engine
BSFC	Brake specific fuel consumption	MBT	Maximum brake torque
CO	Carbon monoxide	NEDC	New European Driving Cycle
CO_2	Carbon dioxide	NOx	Nitrogen oxides
CR	Compression ratio	NYCC	New York city cycle
DI	Direct Injection	OEM	Original equipment manufacturer
DISI	Direct injection spark ignition	RON	Research octane number
EC	Eddy-current	RPM	Revolution per minute
ECU	Engine control unit	SI	Spark Ignition
EGR	Exhaust Gas Recirculation	TDC	Top dead center
EPA	Environmental protection agency	TWC	Three-way-catalyst
EU	European Union	UK	United Kingdom
EUDC	Extra-urban driving cycle	US	United States
FC	Fuel consumption	VCR	Variable compression ratio
FTP-75	Federal test procedure 75	WLTC	Worldwide Harmonized Light Vehicles Cycle
HC	Unburned hydrocarbons	w.r.t	With respect to